Available online at www.sciencedirect.com
SCIENCE DIRECT®
Catalysis Today 96 (2004) 119–126
CATALYSIS TODAY
www.elsevier.com/locate/cattod

Sol–gel preparation and photocatalysis of titanium dioxide

C. Su*, B.-Y. Hong, C.-M. Tseng

Institute of Organic and Polymeric Materials, National Taipei University of Technology, Taipei 106, Taiwan

Accepted 8 June 2004

Abstract

Titanium dioxide (TiO_2) is extensively used as a photocatalyst due to the strong oxidizing power of its holes, high photostability and redox selectivity. In the present work, the microstructural and chemical properties of TiO_2, obtained by a sol–gel procedure, were investigated. TiO_2 sols were prepared by the hydrolysis and condensation of titanium (IV) *n*-butoxide in *iso*-propyl alcohol. The particle dimensions and morphology of the product were examined by transmission electron microscopy (TEM), the crystal structure by X-ray diffraction (XRD) and chemical state was identified by electron spectroscopy for chemical analysis. The titania particles in the initial sol was elliptical in shape. Upon annealing at 400 °C, the TiO_2 particles turned polygonal in shape. The XRD pattern was sensitive to heat treatment. At a calcination temperature of 400 °C, only anatase phase was observed. As calcination temperature was increased to 700 °C, the rutile phase became the major constituent of TiO_2. The XRD data also showed that the crystal size of TiO_2 increased from 4 to 35 nm as the temperature was increased to 700 °C. Simultaneously, the BET surface area recorded a decreased from 122 to 11.5 $m^2\ g^{-1}$. To examine the photocatalytic activity of the as-prepared TiO_2, the photodecomposition of salicylic acid was carried out. It was found that the anatase phase dominated the salicylic acid decomposition under the experimental conditions. A plausible explanation correlating the photocatalytic activity and the TiO_2 preparation conditions is discussed.

Keywords: Titanium dioxide; Sol–gel; Photocatalysis

1. Introduction

Photochemical reactions catalyzed by semiconductors have been investigated extensively in the degradation of toxic organic pollutants [1,2], in organic synthesis [3,4] and in energy conversion and storage [5,6]. In these reactions, photogenerated electrons and holes migrate to the semiconductor surfaces where they can induce reduction and oxidation of adsorbed molecules. Titanium dioxide (TiO_2), for instance, is one of the most popular and promising materials in photocatalytic application due to its strong oxidizing power of its holes, high photostability and redox selectivity [7]. TiO_2 is commercially available and easy to prepare in the laboratory. An important requirement for improving the TiO_2 catalytic activity is to increase its specific surface area, which is certainly dependent on the crystal size. The smaller the catalyst, the larger will be its specific surface area. A number of methods have been used to prepare TiO_2 nanoparticle, such as chemical precipitation [8], microemulsion [9], hydrothermal crystallization [10] and sol–gel [11]. Sol–gel is one of the most successful techniques for preparing nanosized metallic oxide materials with high photocatalytic activities [12]. By tailoring the chemical structure of primary precursor and carefully controlling the processing variables, nanocrystalline products with very high level of chemical purity can be achieved. In sol–gel processes, TiO_2 is usually prepared by the reactions of hydrolysis and polycondensation of titanium alkoxides, $Ti(OR)_n$ to form oxopolymers, which are then transformed into an oxide network. The reaction scheme is usually written as follows:

1. Hydrolysis

$$M(OR)_n + H_2O \rightarrow M(OR)_{n-1}(OH) + ROH$$

2. Condensation
   Dehydration:

$$M(OR)_n + M(OR)_{n-1}(OH) \rightarrow M_2O(OR)_{2n-2} + ROH$$

* Corresponding author. Tel.: +886 2 27712171x2435; fax: +886 2 27317174.
E-mail address: f10913@ntut.edu.tw (C. Su).

0920-5861/$ – see front matter © 2004 Published by Elsevier B.V.
doi:10.1016/j.cattod.2004.06.132

Dealcoholation:

$$2M(OR)_{n-1}(OH) \rightarrow M_2O(OR)_{2n-2} + H_2O$$

the overall reaction is

$$M(OR)_n + \frac{n}{2}H_2O \rightarrow MO_{n/2} + nROH$$

To obtain homogeneous titanium oxide networks for application, control of hydrolysis is essential. Therefore, in addition to the precursor for titanium source, some of the chelating reagents, such as diol, carboxylic acid or diketonate compounds are added [10]. The condensation is usually accomplished by gelization and calcination. Condensation pulls together the constitute particles of the gel into a compact mass, thus building up the metal oxide crystal [13]. Calcination temperature, on the other hand, is especially important for removing the organic molecules from the final products and completing the crystallization. However, very high calcination temperature results in aggregation and/or phase transformation, and affects the microstructures as well as the properties of TiO_2 nanoparticles. It has been established that the photocatalytic activity of TiO_2 strongly depends on its crystal structure. For instance, anatase-phase TiO_2 crystallites are generally found to be more active than rutile [14]. Rutile phase has also been shown to be more active than anatase in few examples, such as photodecomposition of H_2S [15] and photooxidation of H_2O with Fe^{3+} [16]. Recently, it was found that anatase/rutile mixture (7/3) made the best photocatalyst for the oxidation of organic materials in the wastewater treatment [17]. Thus, the microstructure of the TiO_2 plays crucial role in determining its photocatalytic activity [18].

The aim of this work is to study the correlation between photocatalytic activity of TiO_2 powders and its several properties, including crystal structure, surface area, particle size and possible reaction site on the surface of TiO_2. The nanocrystalline TiO_2 powders were prepared from titanium (IV) *n*-butoxide via sol–gel synthesis. The effect of various preparation conditions on the microstructural evolution, surface area and photocatalytic capability of the TiO_2 powders was investigated. To examine the photocatalytic efficiency of the synthesized TiO_2, photodecomposition of the salicylic acid, a prototype molecule, was studied. It has been reported that salicylic acid is degraded in aqueous dispersions of TiO_2 under UV illumination [19,20]. The advantageous spectral characteristics of salicylic acid favor the monitoring of its decomposition upon illumination simply by measuring the concentration changes.

2. Experimental

2.1. Sol–gel synthesis of TiO_2

The TiO_2 was prepared using a sol–gel method, with some modifications, that was used by Liang [21] for preparation of TiO_2 thin film. A solution of titanium (IV) *n*-butoxide (Ti(*O*-Bu)$_4$,) in isopropyl alcohol (*i*-PrOH), was used as molecular precursor of TiO_2. In order to control the reaction kinetics, acetylacetone (acac) was used as a chemical additive to moderate the reaction rate. All chemicals obtained from Aldrich and Merck were used as received. Water was deionized. The water used for hydrolysis in solution with *i*-PrOH was added gradually under mechanical stirring. The reaction condition was carefully controlled to obtain white precipitate of titanium oxyhydroxide, which was then washed with water for several times. The molar ratio of these reactants was: Ti(*O*-Bu)$_4$:H_2O:*i*-PropOH:acac = 1:100:2:0.01. The final solution was peptized by adding HNO_3, followed by refluxing at 85 °C for 8 h to give a sol of pH ~2.5. During optimization of processing conditions in the early stage of this work, the important role of the pH value in the control of the size of the TiO_2 particles was revealed. A portion of as-prepared titania hydrosol was retained for further analysis and comparison. The other portion was gelled by drying at 100 °C for 3 h, then calcinated in vacuum oven (1 Pa; NeyTech Qex-JFF 2000) at various temperatures (400–700 °C) to give TiO_2 powder. The experimental procedure is shown schematically in Fig. 1.

2.2. Characterization of sol–gel-synthesized TiO_2

The above-prepared TiO_2 samples were characterized for microstructural properties by transmission electron microscopy (TEM; Hitachi, H-7100). The Brunauer, Emmett and Teller (BET) surface area was obtained from nitrogen adsorption–desorption data (Micromeritics, ASAP-2010). The chemical composition was verified using the electron spectroscopy for chemical analysis (ESCA; VG Scientific ESCALAB 250). The crystalline phase was determined by X-ray diffraction (XRD; Japan MAC Science, MXP 18). All peaks measured by XRD analysis were assigned by comparing with those of JCPDS data [22]. The crystal size of the TiO_2 during different states of heat treatment was obtained by the XRD line profile analysis. The zeta potential of some of the sol solutions was measured using zeta potential analyzer (Brookhaven Instruments Co.). The average size of the TiO_2 particles was acquired by dynamic light-scattering measurement (DLS; BI-MAS Particle Sizing).

2.3. Photocatalysis by sol–gel-synthesized TiO_2

The photocatalytic reaction was carried out in a custom-made photoreactor (FanChun Technology Inc., PR-2000) as shown in Fig. 2. The system is open to air with total sixteen light tubes circulating the reaction cell made by quartz. The UV light was obtained from UV-lamps (wavelength 253.7 ± 0.8 nm) (Germicidal Lamp, Sankyo Denki Co., Ltd.). The power at the position of the reactor center, measured in the air by a power meter (Molectron, PM 150x), was about (1.2 ± 0.2) mW cm^{-2}. UV–vis spectrometry (Hitachi, U-2001)

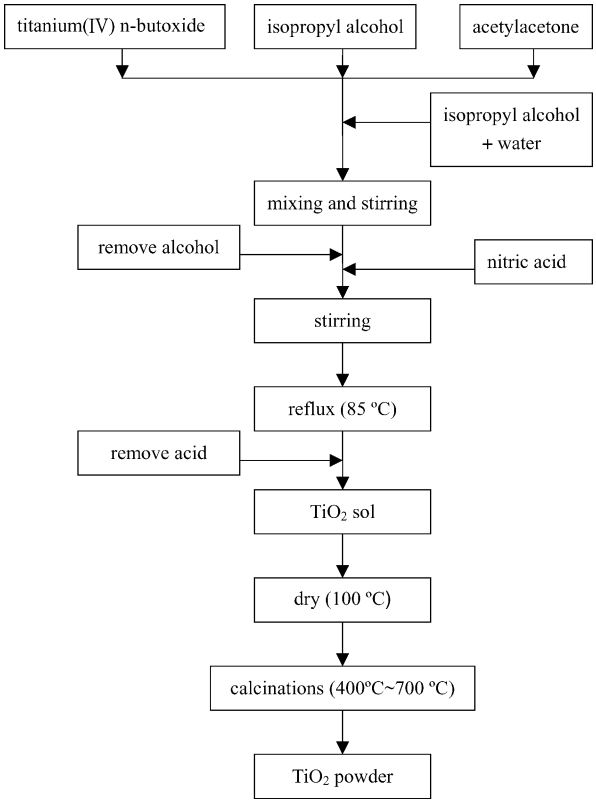

Fig. 1. Flow chart of the method of preparation of TiO_2 sample by sol–gel synthesis.

was used to monitor the absorbance spectra of salicylic acid as a function of illumination time. Before the photoreaction experiment, the aqueous solution of salicylic acid, 4×10^{-4} mol/l (M), was stirred in the presence of TiO_2 sample in the dark for at least 30 min to ensure the complete equilibrium of adsorption process. During illumination, the solution was bubbled with nitrogen gas. The photocatalytic efficiencies of the TiO_2 samples prepared by applying various calcination temperatures were compared and the results were fitted by combination of two first order reaction models.

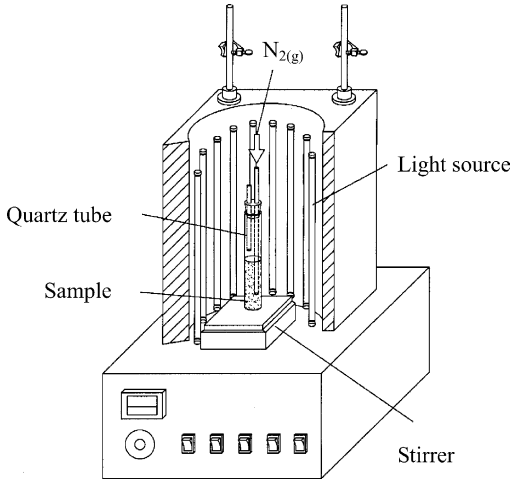

Fig. 2. Drawing of the photoreactor for the study of salicylic acid photodecomposition.

3. Results and discussion

3.1. Preparation and characterization of TiO_2 samples

3.1.1. pH-dependent TiO_2 sol stability

Solid oxides in aqueous suspension generally possess electrical charge due to the amphoteric dissociation of surface hydroxyl groups, the adsorption of H^+/OH^- ions, or metal hydroxo compounds from the hydrolysis of solid material. The resultant surface charge is pH dependent. Bahnemann et al. have reported that the surface acidic/basic properties of TiO_2 can be determined by chemisorption of H^+ ($TiO_2 + nH^+ \leftrightarrow TiO_2H_n^{n+}$, for pH $<$ 3.5) or OH^- ($TiO_2 + nOH^- \leftrightarrow TiO_2(OH)_n^{n-}$, for pH $>$ 3.5) [14,23]. The strong repulsive force among charged particles reduces the probability of coalesce and thus more stable sols can be formed in acidic or alkaline media. We first optimized the pH value of the TiO_2 sol dispersion medium. The pH was controlled by the addition of HNO_3 and NH_4OH. As shown in Fig. 3, the surface potential of TiO_2 increases in general as the pH decreases. The measured isoelectric point is about 5–7, consisting with the reported data that indicate the isoelectric point of TiO_2 varies within a pH range of 5–6.8. Away from the isoelectric range, the less aggregated TiO_2 sol should be formed. Fig. 4 shows the average size of TiO_2 particle as a function of pH value. The zone of maximum particle size is located within the pH range 5–8, which practically coincides with the pH value of TiO_2 isoelectric point. It was noted that in this pH range, the sol became milky-white, accompanied by precipitation. This observation indicated the rapid coagulation of TiO_2 particles as suggested by the pH dependent surface potential. For pH $<$ 3 and/or pH $>$ 9, clear sol with nanosized TiO_2 was obtained. In this work, we choose nitric acid as a sol stabilizer to obtain an acidic media with pH $<$ 2 for TiO_2

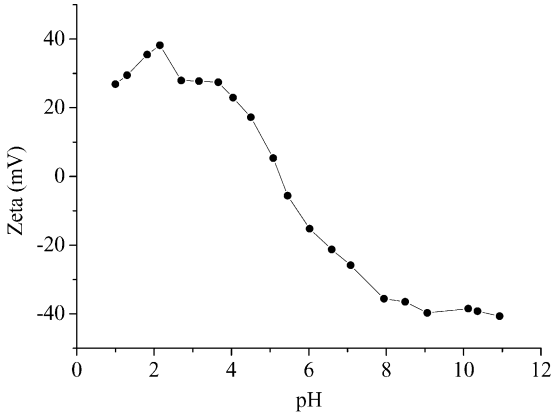

Fig. 3. The pH-dependent TiO_2 surface potentials.

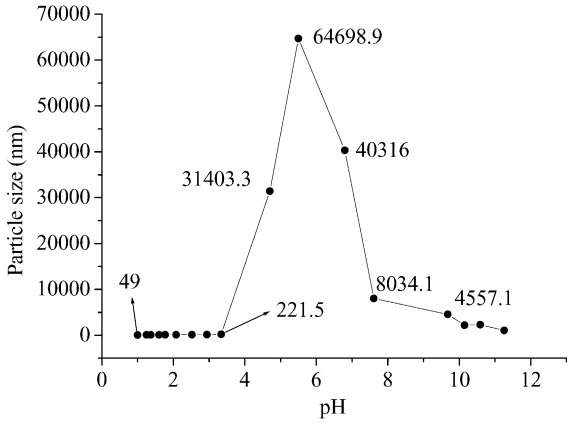

Fig. 4. The pH-dependent TiO_2 particle size.

synthesis. The sols prepared using this method can be stabilized for a period longer than a year.

3.1.2. TEM analysis

TEM is a useful technique for the analysis of the size and shape of ultrafine particles. The crystal growth in different stage of sol–gel process was analyzed by TEM. Fig. 5 shows the TEM micrographs at various growing stages of sol–gel synthesis of TiO_2. As shown in Fig. 5, the TiO_2 particles grew step by step. In the first step of newly formed gel, the shape of the TiO_2 was observed as elliptical (Fig. 5a) with average length of ~25 nm. At the middle stage, after the gel was dried by removing the liquid phase, the micrograph (Fig. 5b) exhibits irregular polyhedron aggregates composed of elementary particles of the size ranging from 30 to 40 nm. Such geometry for the anatase phase [14] is consistent with the XRD result (Section 3.1.3). Upon annealing at 400 °C for 2 h, agglomerates of big but irregular TiO_2 particles with the size of as large as 250 nm (Fig. 5c), consisting with the particle size measurement by light scattering techniques (Section 3.1.3), were produced. The discrete TiO_2 particles were packed together in rather open structure. Similar structure was observed by Barringer et al. for isopropoxide-derived TiO_2 powder prepared by vacuum-dried at 160 °C and sintered in air at 800 °C [24]. Distribution of particle size of TiO_2 over a broad range was observed (Fig. 5c), suggesting that the crystallization to the anatase structure upon calcination might have gone through the solid-state epitaxial crystal growth with a slow nucleation process [14]. The original gel structure affects structural evolution in all subsequent processing steps. It is known that the TiO_2 crystals grow from TiO_6 octahedra that are terminated by the surface Ti–OH groups. In Fig. 5(a), the elliptical shaped initial state of TiO_2 shows characteristic of octahedral configuration with two pointed sharp ends. Under acidic condition, the surface hydroxyl groups can be protonated to form $Ti–OH_2^+$, which then combines readily with another Ti–OH to form Ti–O–Ti oxygen bridge by eliminating a water molecule [14] and simultaneously releasing one proton ion. In this work, slow nucleation in the crystal

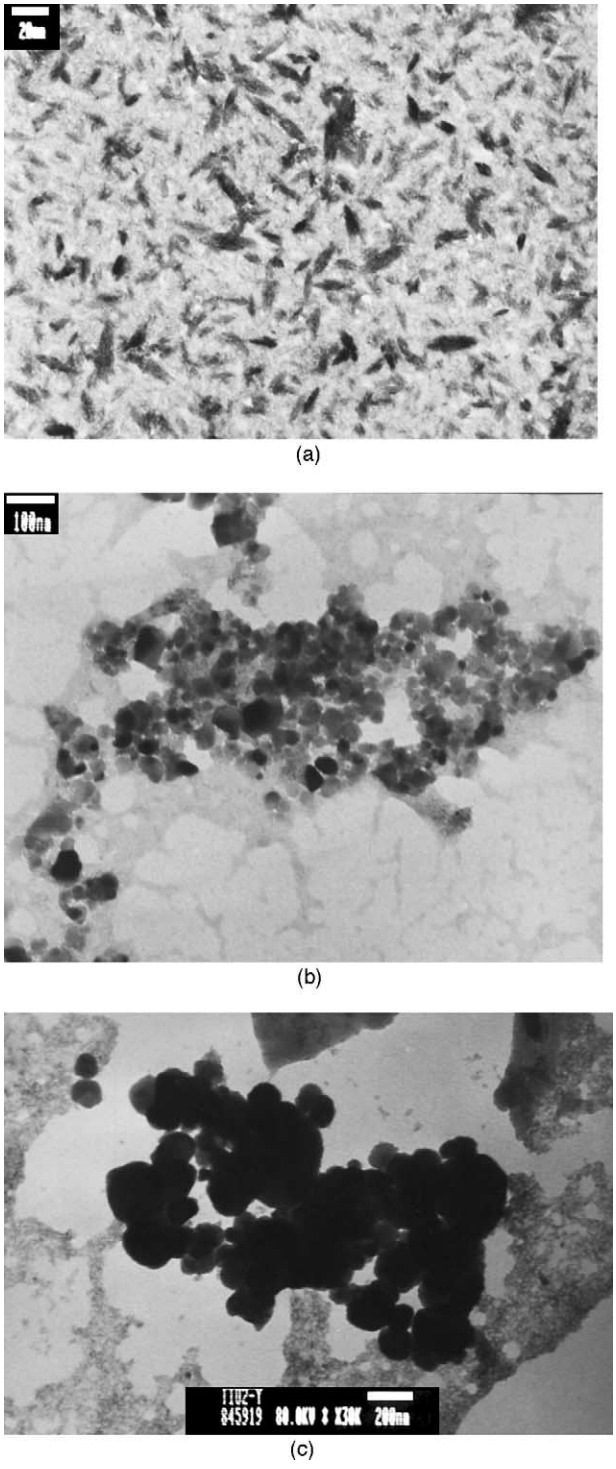

Fig. 5. TEM photograph of (a) TiO_2 hydrosol, (b) dried TiO_2 hydrosol, (c) sample from TiO_2 hydrosol calcinated at 400 °C for 2 h.

growth and the irregular surfaces of final TiO_2 particles aroused due to the poor nucleophilicity of the nitrate anion. The water condensation process may occur between faces of TiO_6 octahedra (face-sharing mechanism), leading to the formation of anatase phase, or between edges of TiO_6 octahedra (edge-sharing mechanism), leading to the formation of rutile phase [14]. The results from XRD and TEM

revealed that the face-sharing mechanism may dominate the grain growth of TiO_2 in the early stage. At higher temperature, the phase transition proceeds by rearrangement of the octahedral.

3.1.3. XRD, ESCA and BET analysis

The crystal phase of TiO_2 was analyzed by XRD. TiO_2 particles prepared by hydrolysis and condensation were amporphous as no distinct XRD pattern was found (not shown). After refluxing and drying of stable sol, the partial crystallization occurred as shown in Fig. 6(a). The structure phases observed were all anatase. Higher temperature increases the tendency of crystal growth; hence, to achieve complete crystallization, dry-gel TiO_2 powders were calcinated at different temperature (T_c). However, it is to be noted that calcination unavoidably led to sintering of the nanocrystallites as demonstrated by the TEM images. The XRD patterns of the TiO_2 samples after heat treatment at 400, 500, 600 and 700 °C for 2 h is, respectively, shown in the Fig. 6(b–e). Obviously, the amorphous phase crystallizes to the anatase structure at temperature of 400 °C, at which all the residual organics are believed to be liberated completely based on TGA data (not shown). However, a phase transformation from anatase to rutile (A → R) also aroused upon increasing the calcination temperature. When the TiO_2 was heated up to 500 °C and above, the products became a mixture of anatase and rutile. Anatase phase is in fact a metastable polymorph of TiO_2 with respect to rutile [25,26]. It is known [27] that thermal treatment and surface defects are two important factors in TiO_2 phase transformation. The primary formed TiO_2 particles usually contain large portion of defect sites, high temperature facilitates bond breaking as well as atoms rearrangement and therefore the A → R occurs easily. On the other hand, A → R transformation is initiated by forming the rutile nuclei along the anatase {1 1 2} twin interface, which has the structural similarity to rutile and thus the rutile structure develops directly at the expense of anatase crystallites [14]. Energetically, critical size of anatase is required for A → R transformation to occur. Upon heating (see below), the anatase TiO_2 crystals grow significantly to effect this transformation.

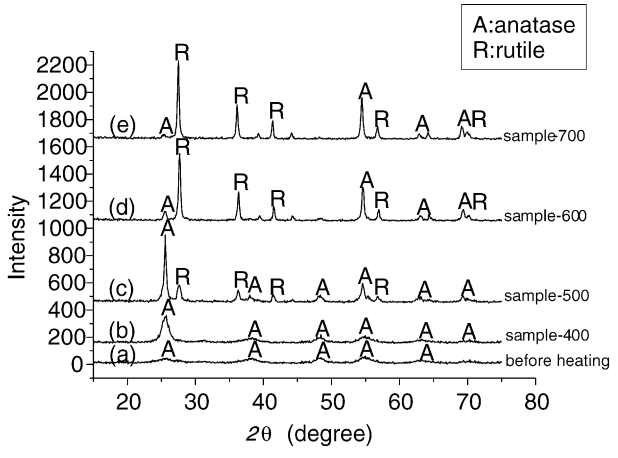

Fig. 6. XRD patterns of sol–gel-synthesized TiO_2 (a) before and after thermal treatment at (b) 400 °C, (c) 500 °C, (d) 600 °C and (e) 700 °C for 2 h.

To quantify the crystal size of TiO_2, the d spacing at 3.52 Å (1 0 1) phase for anatase and 3.25 Å (1 1 0) phase for rutile were used. X-ray peak-broadening was analyzed by employing the Scherrer equation: $L = \kappa\lambda/\beta \cos\theta$, where L is the length of the crystal in the direction of the d spacing, κ is a constant of 0.9, λ is the wavelength of the radiation used (1.5405 Å), β is the full width at half-maximum (FWHM) of selected peak and θ is the Bragg's angle of diffraction for the peak. The relative abudance of anatase to rutile was calculated from the equation of $F_r = 1.26\, I_r/(I_a + 1.26\, I_r)$, where I_r and I_a are the strongest intensities of rutile (1 1 0) and anatase (1 0 1) peaks, respectively [10,28]. The average crystal sizes of TiO_2 before and after annealing at various temperatures are listed in Table 1. It is apparent that thermal annealing greatly affects the structure and the size of the resulting TiO_2 crystal. The crystal sizes for both anatase and rutile increased with increasing of calcination temperature, indicating aggregation of TiO_2 nanoparticles upon annealing. The fraction of rutile becomes greater with increasing reaction temperature, consistent with the previous result that increasing the temperature of heat treatment accelerates phase transformation from thermodynamically metastable anatase to most stable and more condense rutile phase. As mentioned earlier, the hydrous gel contains minute-sized TiO_2 crystal with hydroxyl groups (–OH) on the surface. During the heat treatment, the dehydration occurs and so the crystals grow to a size larger than those of the original particles.

The above XRD pattern indicates formation of TiO_2 crystals that can be confirmed by the ESCA measurement. Fig. 7 shows an ESCA survey spectrum of TiO_2 sample. The peaks appearing in this spectrum include the Ti_{2P} doublet, O_{1s}, O Auger peaks and the C_{1s} peaks, etc. The spectrum is in good agreement with the standard spectrum of TiO_2. All the binding energies were referenced to C_{1s} at 284.5 eV.

BET adsorption of nitrogen gas for surface area determination at the temperature of liquid nitrogen was performed on TiO_2 samples prepared using sol–gel synthesis, followed by different heat treatment. For the comparison, the surface area of degussa P-25 was also acquired under the same experimental condition. The results

Table 1
Results of XRD measurements for TiO_2 samples

Calcination temperature (T_c) (°C)	Diffraction angle (2θ)	FWHM (radian)	Crystal size (nm)	A/R
Before annealing (A)	25.55	0.037520	4.10	
400 (A)	25.64	0.011010	13.96	9.8
500 (A)	25.65	0.008740	17.60	3.23
500 (R)	27.51	0.008323	18.78	
600 (A)	25.46	0.007426	20.68	0.12
600 (R)	27.51	0.005941	26.31	
700 (A)	25.56	0.005812	26.44	0.03
700 (R)	27.44	0.004455	35.07	

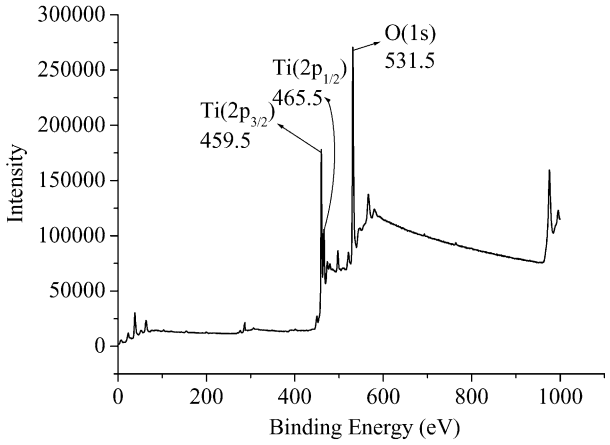

Fig. 7. An ESCA survey spectrum of the TiO_2 sample.

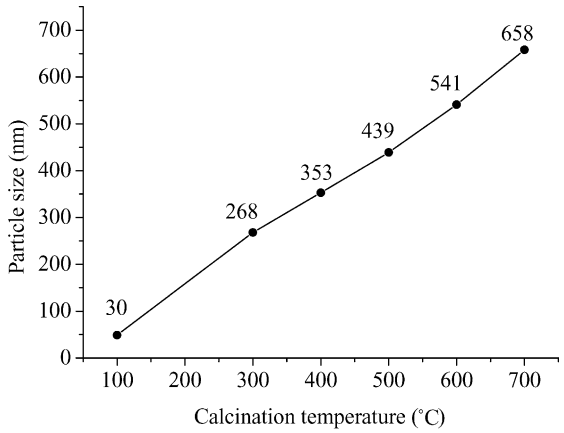

Fig. 8. The DLS-measured TiO_2 particle size as a function of calcination temperature.

listed in Table 2 show the dependence of the surface area on the temperature of calcination of the TiO_2 samples. It can be seen that the specific surface area shift towards smaller values at higher calcination temperatures. Samples calcinated at 400 °C possess high specific surface area (122 $m^2\ g^{-1}$ according to BET), which then decreased appreciably to 11.5 $m^2\ g^{-1}$ with increasing the calcination temperature up to 700 °C. This observation indicates an increase in the crystal size of TiO_2 in increasing the calcination temperature. The TiO_2 particle size was also measured by dynamic light scattering (DLS) technique. Fig. 8 shows the variation of TiO_2 particle size (measured by DLS) as a function of calcination temperatures, which is in good agreement with the BET results.

3.2. Photocatalytic activity

The decomposition of organic molecules that occurs under irradiation of above synthesized TiO_2 is of great importance. In the present work, the degradation of salicylic acid was selected as a test reaction to verify the photocatalytic activity of different TiO_2 dispersion samples. The photodegradation was studied by monitoring the absorbance of the salicylic acid solution at the absorption maximum (wavelength of 296 nm) of the aromatic acid moiety. Fig. 9 plots the concentration changes of salicylic acid as a function of illumination time of the TiO_2 samples prepared by calcinating at different temperatures (T_c): 400, 500, 600 and 700 °C (sample-400, sample-500, sample-600 and sample-700). The control experiments showed that salicylic acid could decompose scarcely in the absence of TiO_2 under the same irradiation condition, indicating that the presence of TiO_2 played an important role in the photodegradation of salicylic acid. The photocatalytic activity of Degussa P25 (not shown), measured by photodegradation of salicylic acid, is similar to that obtained from sample-600. Results in Fig. 9 show that varying the calcination temperature changes the photocatalysis efficiency of TiO_2 significantly. Several factors, including the total surface area, crystal composition, crystal phase and catalyst morphology contribute to the altered catalytic performance. Anatase is usually believed to be more photocatalytically active than the rutile phase [2,20]. It is found that TiO_2 photocatalysis efficiency increases with the T_c up to 500 °C reaching a maxima, i.e. sample-500 is the most active to catalyze the photodecomposition of salicylic acid. The sample-700 showed only little photocatalysis efficiency to decompose salicylic acid. The deterioration of photocatalysis efficiency may be due to the phase

Table 2
Surface area of TiO_2 samples

Calcination temperature (°C)	Surface area ($m^2\ g^{-1}$)
400	122.2
500	65.7
600	26.9
700	11.5
Degussa P-25[a]	52.0

[a] The standard Degussa P-25 TiO_2 sample.

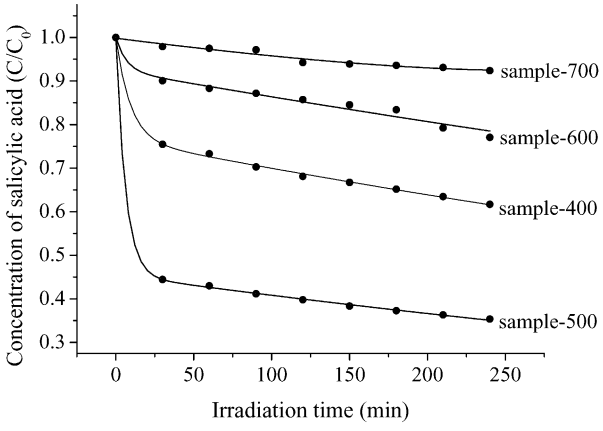

Fig. 9. Photodecomposition of salicylic acid for the TiO_2 prepared by calcinating at different temperatures, viz. 400, 500, 600 and 700 °C, plotted as salicylic acid absorbance at a wavelength of 296 nm as a function of illumination time.

transformation from anatase to rutile after high temperature treatment. In addition, the larger-sized TiO_2 crystal (Table 1) resulted from high temperature aggregation also abated its photocatalytic ability. Sample-400 possessed the largest surface area and it is composed primarily of anatase phase. Nevertheless, the broad XRD feature for sample-400 as shown in Fig. 6(b) indicated that anatase crystallization of TiO_2 treated at 400 °C was incomplete. The amorphous titania is known to have very low photocatalytic efficiency compared to that of the anatase or rutile phase due to an increased electron-hole recombination rate [7], hence the sample-400 was expected to exhibit lower photocatalysis efficiency than that of the sample-500.

It is to be noted that each data set in Fig. 9 was determined in a separate experiment, i.e. using the newly prepared TiO_2, the values for peak area are subject to about 15–20% variability. Within this uncertainty, the concentration changes of salicylic acid versus irradiation time showed similar behavior as observed for a series of TiO_2 samples, and was confirmed by several replicate experiments. The changes in salicylic acid concentration were found to show a rapid decrease in the aqueous TiO_2 dispersion for the initial illumination. After prolonged irradiation, the rate of decay of salicylic acid became less. To derive kinetic information, the decay of absorption due to the decomposition of salicylic acid was tentatively assumed to follow the Langmuir–Hinshelwood kinetics (L–H) model with the rate being proportional to the coverage of reactant on the catalyst surface. Since the initial concentration of salicylic acid is low ($c_0 = 4 \times 10^{-4}$ M), the reaction rate becomes apparent first order:

$$\text{Rate} = -\frac{\mathrm{d}[C]}{\mathrm{d}t} = k_\mathrm{a}[C] \quad (1)$$

k_a is the apparent rate constant and $[C]$ is the concentration of salicylic acid. To determine the reaction rate constant, curves of the variation of concentration of salicylic acid as a function of illumination time need to be fit into the Eq. (1). However, to produce a good fit to the experimental data, we have to incorporate two channels for disappearance of salicylic acid. The decay curve of time dependent concentration of salicylic acid can be described satisfactory by summation of two first-order exponential functions of the form (Eq. (2))

$$\frac{[C]}{[C_0]} = \theta_1 \exp[-k_1 t] + \theta_2 \exp[-k_2 t] \quad (2)$$

k_1 and k_2 represent the apparent rate constants of the pseudo-first order for removal of salicylic acid under the illumination from two different channels (designated to fast and slow channel) for salicylic acid, possibly corresponding to two surface reaction sites with initial coverage of θ_1 and θ_2, where $\theta_1 + \theta_2 = 1$. $[C_0]$ and $[C]$ are the concentrations of salicylic acid, respectively, before and after irradiation time t. As shown in Fig. 9, sample-400 to sample-700, the lines through the data points of concentrations of salicylic acid display the resultant curves from the fitting. The values of rate constants k_1 and k_2, and the corresponding coverage θ_1 and θ_2, calculated in this way are given in Table 3. Rate constants from curve of sample-700 are difficult to be accurately determined due to the insufficient photoactivity in this particular system. Remarkably, the coverage associated with these two channels varies with calcination temperatures. The differences in the terms of the chemical properties and structures of these two reaction centers can not be absolutely determined in the present experiments. The changes in the photocatalytic efficiency over the range of calcination temperatures are accompanied by the changes in the phase composition of sol–gel-prepared TiO_2. At the higher calcination temperatures (above 500 °C), the photocatalytic activity decreases that is probably associated with the decrease in anatase fraction. Therefore, it is possible that the fast and slow reaction channels might correspond to the salicylic acid adsorption/reaction at the reaction sites on the anatase and rutile phase of TiO_2. Tunesi et al. [29] and Kratochvilova et al. [30] have studied the reactions of salicylic acid with TiO_2 and found that salicylic acid forms a complex with the surface titanium atom which is the most chemically active site with incomplete coordination sphere on the anatase crystal. Complex formation connotes more direct interaction between catalysis substrate and the contact adsorbate, and therefore facilitates the hole transfer which is the most important step in the mechanism of photocatalysis. Alternatively, in the absence of the anatase phase as well as surface complexation, the decomposition of salicylic acid has to proceed via the less direct route of the generated intermediates, i.e. the $^{\bullet}$OH radical [20]. The above-mentioned two reaction routes indeed follow substrate-mediated excitation mechanism. Another possible pathways for photo-induced surface reaction is so called direct adsorbate excitation mechanism in which direct excitation of salicylic acid on TiO_2 can also lead to a variety of photochemical processes. Based on the absorption spectrum, the irradiation wavelength (253.7 nm) used in the photodecomposition of salicylic acid is about its absorption minimum, and therefore, it is unlikely that the adsorbate excitation played an important role in the present case. Further, quantitative determination of the wavelength-dependent reaction rates may clarify this point.

Table 3
Photocatalytic activities of TiO_2 samples

Calcination temperature (°C)	Coverage θ_1	Rate constant k_1 (min^{-1})	Coverage θ_2	Rate constant k_2 (min^{-1})
400	0.22	1.3×10^{-1}	0.78	1.1×10^{-3}
500	0.54	1.8×10^{-1}	0.46	1.1×10^{-3}
600	0.13	1.6×10^{-1}	0.87	3.0×10^{-4}
700	0.08	6.0×10^{-3}	0.92	7.4×10^{-5}

4. Conclusion

This work demonstrates that a sol–gel process, originally designed for depositing TiO_2 thin film, can be applied to prepare TiO_2 powders that possess good photocatalytic activity in decomposition of salicylic acid. Titanium (IV) *n*-butoxide can be an effective precursor for synthesis of TiO_2. Stable sol can be obtained under the acidic condition with pH < 2. The experimental conditions and heat treatment after preparation can be optimized to obtain the desired composition and microstructure. Anatase nucleates, as initial kinetic product, grows first. Increasing the calcination temperature induces phase transformation from anatase phase to thermodynamically more stable rutile phase. The fraction of rutile phase becomes greater with increasing calcination temperatures. It can be concluded from the measurement of TEM, BET and DLS that an increase in the particle size of TiO_2 is associated with the increase in the calcination temperatures. Calcination temperatures used in sol–gel preparation of TiO_2 samples significantly affect the photocatalysis efficiency of samples in the photodecomposition of salicylic acid. This may be due to the heat-induced TiO_2 aggregation and phase transformation. The photodegradative reactions of salicylic acid may be following either fast or slow reaction channels, possibly corresponding to the anatase or rutile reaction sites on TiO_2 surface.

Acknowledgement

We gratefully acknowledge the financial support of the National Science Council of the Republic of China (Grant: NSC 92-2113-M-027-001) for this research. The stimulating discussion with Prof. S.-T. Chiang and Prof. C.-G. Wu is gratefully acknowledged.

References

[1] P.V. Kamat, Chem. Rev. 93 (1993) 267.
[2] M.R. Hoffmann, S.T. Martin, W. Choi, D.W. Bahnemann, Chem. Rev. 95 (1995) 69.
[3] H. Kisch, J. Prakt. Chem. 336 (1994) 635.
[4] M.A. Fox, M.T. Dulay, Chem. Rev. 93 (1993) 341.
[5] A.J. Bard, Science 207 (1980) 139.
[6] A.J. Bard, J. Phys. Chem. 86 (1982) 172.
[7] B. Ohtani, Y. Ogawa, S. Nishimoto, J. Phys. Chem. B 101 (1997) 3746.
[8] A. Scolan, C. Sanchez, Chem. Mater. 10 (1998) 3217.
[9] M. Lal, V. Chhabra, P. Ayyub, A. Maitra, J. Mater. Res. 13 (1998) 1249.
[10] M. Wu, G. Lin, D. Chen, G. Wang, D. He, S. Feng, R. Xu, Chem. Mater. 14 (20021974) 1974.
[11] C.-C. Wang, J.Y. Ying, Chem. Mater. 11 (1999) 3113.
[12] R.S. Sonawane, S.G. Hegde, M.K. Dongare, Mater. Chem. Phys. 77 (2002) 744.
[13] N.-L. Wu, Bull. Coll. Eng., N.T.U. 84 (2002) 85.
[14] H. Yin, Y. Wada, T. Kitamura, S. Kambe, S. Murasawa, H. Mori, T. Sakata, S. Yanagida, J. Mater. Chem. 11 (2001) 1694.
[15] D.D. Beck, R.W. Siegel, J. Mater. Res. 7 (1992) 2840.
[16] T. Ohno, D. Haga, K. Fujihara, K. Kaizaki, M. Matsumura, J. Phys. Chem. B 101 (1997) 6415.
[17] R.J. Berry, M.R. Mueller, Microchem. J. 50 (1994) 28.
[18] X.-Z. Ding, X.-H. Liu, Mater. Sci. Eng. A 224 (1997) 210.
[19] O. Legrini, E. Oliveros, A.M. Braun, Chem. Mater. 93 (1993) 671.
[20] J.H. Schattka, D.G. Shchukin, J. Jia, M. Antonietti, R.A. Caruso, Chem. Mater. 14 (2002) 5103.
[21] N.-Y. Liang, Master Thesis, National Central University, Taiwan, 1999.
[22] JCPDS Data, 21-1272.
[23] D. Bahnemann, A. Henglein, L. Spanhel, Faraday Discuss. Chem. Soc. 78 (1984) 151.
[24] E.A. Barringer, H.K. Bowen, Commun. Am. Ceram. Soc. (1982) 199.
[25] B.L. Bischoff, M.A. Anderson, Chem. Mater. 7 (1995) 1772.
[26] A. Navrotsky, O.J. Kleppa, J. Am. Ceram. Soc. 50 (1967) 626.
[27] W.W. So, S.B. Park, K.J. Kim, S.J. Moon, J. Colloid Interface Sci. 191 (1997) 398.
[28] A.G. Gaynor, R.J. Gonzalez, R.M. Davis, R. Zallen, J. Mater. Res. 12 (1997) 1755.
[29] S. Tunesi, M. Anderson, J. Phys. Chem. 95 (1991) 3399.
[30] K. Kratochvilova, I. Hoskovcoca, J. Jirkovsky, J. Klima, J. Ludvik, J. Electrochim. Acta 40 (1995) 2603.